Modified annealing approach for preparing multi-layered hematite thin films for photoelectrochemical water splitting

Pannan I. Kyesmen[1], Nolwazi Nombona[2] and Mmantsae Diale[1]
[1]*Department of Physics, University of Pretoria, Private Bag X20, Hatfield 0028, South Africa*
[2]*Department of Chemistry, University of Pretoria, Private Bag X20, Hatfield 0028, South Africa*

Corresponding author e-mail addresses: pannan.kyesmen@up.ac.za; mmantsae.diale@up.ac.za

Abstract
Multi-layered hematite (α-Fe_2O_3) films were prepared on fluorine-doped tin oxide (FTO) using the dip coating method. The first three layers of the films were annealed at 500°C and fourth layers at 500, 600, 700, 750 and 800°C respectively, and their photoelectrochemical (PEC) performance was investigated. Films annealed at 750°C recorded the best performance, producing 0.19 mA/cm^2 photocurrent at 1.23 V vs reversible hydrogen electrode (RHE); 5.3 times more than what was recorded for films sintered at 500°C, and the onset potential yielded a cathodic shift of 300 mV. The enhanced performance was linked to improved crystallization, absorption coefficient, lowered flat band potential, increased charge carrier density, decreased charge transfer resistance at the solid/liquid interface and increased surface states capacitance for films annealed at 750°C. The PEC performance of multi-layered α-Fe_2O_3 films could be improved by annealing the last layers at elevated temperatures without damaging the conducting substrates.

Keywords: hematite, multi-layered films, dip coating, annealing temperature, photoelectrochemical performance

1 Introduction

Hematite, a thermodynamically stable phase of iron oxide has received significant attention in recent years for its potential application in photocatalysis. It is environmentally friendly, abundant and able to absorb considerable photons in the visible part of the electromagnetic spectrum due to its bandgap ranging from 1.9-2.2 eV [1]. However, some of the main challenges that is restricting hematite's use for photocatalysis is its poor conductivity and low absorption coefficient which requires films with thickness of 400-500 nm for sufficient light absorption [1, 2]. Preparation of multi-layered coatings with individual layers sintered at high temperatures had been shown to favour columnar grain growth, increasing crystal size, film density and consequently electron mobility [3-6]. The improvement in electron mobility has been associated to decreased scattering centres and reduction in the mean free path for electrons as a result of large crystallites [3, 5], lowering the film resistivity, thus improving conductivity according to equation 1:

$$\rho = \frac{1}{n_e \mu_e} \quad (1)$$

where ρ represent resistivity, n_e is the number of electrons and μ_e is electron mobility [3].

The multi-layered approach has been employed for preparing hematite photoanodes for photocatalysis [7-9]. Multi-layered hematite films consisting of four layers have been produced for PEC application by sintering iron oxyhydroxide films at 500°C for 120 min [8, 10]. Zhang *et al*, (2014), prepared five stacked layers of hematite films on FTO for PEC water splitting by

annealing at 450°C for a period of 30 min for each layer [7]. In another study, Gonglaves *et al*, [9] prepared hematite films for PEC water splitting by annealing magnetite on FTO at 820°C for 20 min and repeating the procedure to obtain multi-layered films. The preparation of multi-layered hematite films for photocatalytic applications have mostly been done at a fixed annealing temperature for all the layers.

Annealing temperature serves a vital role in influencing the properties and photocatalytic efficiency of hematite films irrespective of the preparation method [11]. Many leading preparation approaches demands, as prerequisite post-deposition sintering temperature between 400-550°C for the production of hematite films [12-16]. However, preparing hematite films at elevated temperatures between 700-800°C for 15-30 min has been reported to improve performance in PEC water splitting [11]. Heating the films at elevated temperatures for longer periods can significantly increase the resistance of FTO and offset desired effects such as increasing crystallization [17]. For multi-layered films, annealing of each layer at elevated temperatures could lead to the deformation of the substrate. Preparation of stacked hematite films at 400-550°C while annealing the last layer at elevated temperatures could improve their properties for enhanced PEC performance without damaging the substrates.

In this work, we prepared four stacked layers of hematite films on FTO substrates by annealing the first three layers at 500°C. Thereafter we investigated the impact of treating the last layers at 500, 600, 700, 750 and 800°C on their PEC performance. The results revealed that hematite films treated at 750°C had the best photocurrent and onset potential at 1.23 V vs RHE. The enhanced performance was linked to improved crystallization and absorption coefficient, lowered flat band potential, increased density of charge carriers, decreased resistance to charge transfer at the solid/liquid interface and increased capacitance of the surface states for films annealed at 750°C.

2 Experimental

2.1 Precursor complex preparation

A solution-based procedure previously described [18] was adopted for preparing the precursor solution. A mixture of 28 g of iron(III) nitrate nonahydrate ($Fe(NO_3)_3.9H_2O$) and 19 ml of oleic acid was heated for 2.5 hrs at 110°C, yielding a red-brown mass. 80 ml of tetrahydrofuran was then used to treat the mass obtained. An ultrasonic bath was used to sonicate the mixture for 15 min and centrifuged for 3 min at 5000 rpm. The supernatant was recovered and used for dip coating of thin films on FTO substrates.

2.2 Dip coating process

FTO substrates cleaned using acetone, ethanol and distilled water and dried with nitrogen gas were used for the preparation of hematite films. Deposition of the precursor solution on FTO was done using a dip-coater at withdrawal velocity of 50 mm/min. Four stacked hematite film layers were prepared on FTO, after drying at 70°C for 15 mins and annealing at 500°C for 2hr (30 mins for each layer). Additional films were prepared under similar conditions except for the fourth layers which were first heated to 500°C, and immediately raised to 600, 700, 750

and 800°C within 5 mins respectively, and annealed at those temperatures for 25 mins. Annealing of the fourth layers at elevated temperatures for a limited time of 25 mins was adopted to avoid the deformation of FTO substrates due to excessive heat. Fig. 1 shows a diagram illustrating the film preparation procedure.

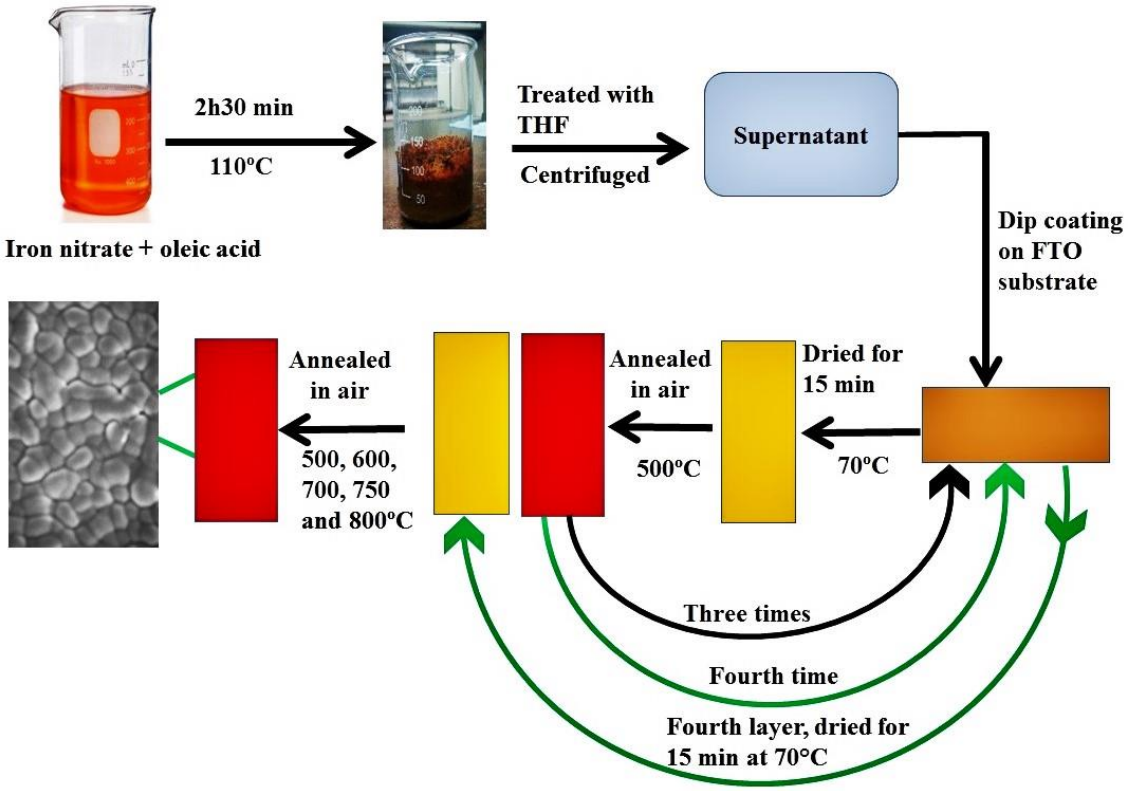

Fig. 1. Schematic illustration of the experimental procedure.

FTO substrates used for the experiments were subjected to the same annealing conditions with the samples prepared to study the impact that such treatments will have on their resistivity. The substrates were first annealed for 1 hr 30 mins at 500°C, after which they were subjected to heat treatment at 500, 600, 700, 750 and 800°C respectively, under the same conditions as the prepared hematite films.

2.3 Characterization

X-ray diffraction (XRD) was employ to examine the structural properties of the films using Bruker D2 PHASER-e diffractometer of Cu-Kα radiation at 0.15418 nm wavelength. Zeiss Crossbeam 540 was to carry out field emission scanning electron microscopy (FE-SEM), to investigate the surface morphology of the films. The Zeiss Crossbeam coupled to energy dispersive X-ray Spectroscopy (EDS) was utilize to check the elements present in the films. Ultraviolet-Visible (UV-Vis) spectroscopy measurements were done with CARY 100 BIO UV-Vis spectrometer to investigate the optical behavior of films. The resistivity of the annealed FTO substrates were studied using a Signatone linear four-point probe.

The PEC performance of the films was studied using VersaSTAT 3F potentiostat from Princeton Applied Research, in a three-electrode electrochemical system with 1M NaOH electrolyte (Ph=13.6). The α-Fe_2O_3 films on FTO, 2 × 2 cm platinum meshed wire and silver/silver chloride (Ag/AgCl) in 3M KCl were used as working, counter and reference electrodes respectively. Approximately, 1.68 cm^2 of the α-Fe_2O_3 photoanode was immersed in the electrolyte. The photocurrent of the films was obtained by carrying out linear sweep voltammetry (LSV) measurements from -0.4 V to 0.7 V vs Ag/AgCl at 0.05 V/s scan rate in dark and under light illumination. The light source was a Newport $Oriel^{®}\ LCS-100^{TM}$ solar simulator calibrated to 1 sun at 100 mW/cm^2 using a Newport 91150V reference cell, and the illumination area of the photoanode was 0.49 cm^2. Mott-Schottky analysis were carried out in dark conditions at a DC potential range of -1.2 to 0.2 V vs Ag/AgCl under a fixed frequency of 1000 Hz and AC amplitude potential of 10 mV. Electrochemical impedance spectroscopy (EIS) measurements of the hematite films were done under illumination at 0.23V vs Ag/AgCl, between 10, 000 to 0.1 Hz frequency range at a potential amplitude of 10 mV. ZView software from Scribner Associates was used to fit the EIS experimental data to an equivalent circuit model. The potential in Ag/AgCl for all the PEC measurements were converted to RHE scale using equation 2 [19],

$$V_{RHE} = V_{Ag/AgCl} + (0.059 \times PH) + V^{\circ}_{Ag/AgCl} \quad (2)$$

where, V_{RHE} is potential in the RHE, $V^{\circ}_{Ag/AgCl}$ = 0.1976 V at 25°C, and $V_{Ag/AgCl}$ represents the potential vs Ag/AgCl reference used during the experiments.

3 Results and Discussion

3.1 Properties of films

3.1.1 Morphology and elemental composition

The surface morphologies of the films examined using FE-SEM are shown in Fig. 2(a-e). The morphologies disclosed spherical nanostructures and the agglomeration of some particles into larva-shaped structures. The surface of the films appeared to be more uniform with increasing annealing temperature. The average particle diameter across the width of the nanostructures was approximated using ImageJ software. FE-SEM cross-sectional images revealed approximate film thickness of about 776 ± 50 nm for the films. Fig. 2(f) shows the cross-sectional image for films sintered at 500°C. Fig. 2(g), (h) and (i) presents the histograms of particle diameter distribution for films sintered at 500, 750 and 800°C respectively, showing their estimated size and standard deviation (SD) values. The particle diameter was observed to increase with temperature to a maximum estimated size of 53.7 nm for films annealed at 750°C, which was 72.1% higher than those of films treated at 500°C. Grain size has been link to the temperature of isothermal growth [20]. At higher temperatures, the atoms gain sufficient diffusion activation energy and are able to migrate with more ease to the grain boundaries to induce grain growth [21]. The observed grain size increase with temperature was due to improved migration of oxygen and iron atoms to grain boundaries leading to their incorporation into the lattice [20, 22]. Decreased in particle diameter was observed for the films sintered at 800°C compared to the ones treated at 750°C. This may be a result of deformation of FTO substrate due to excessive heat which may have interrupted further grain growth [17].

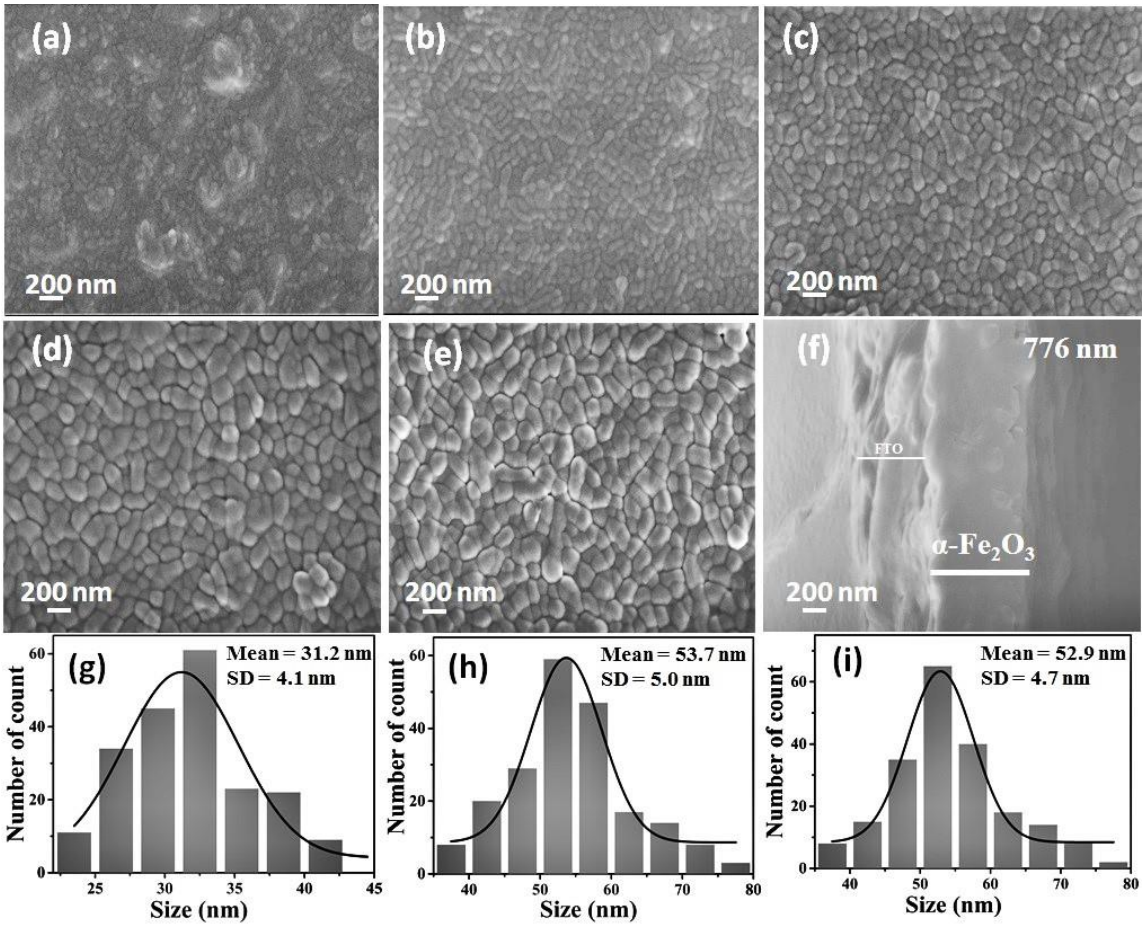

Fig. 2. SEM micrographs for films annealed at (a) 500°C, (b) 600, (c) 700°C, (d) 750°C and (e) 800°C respectively; (f) shows the cross-sectional image for films annealed at 500°C; (g), (h) and (i) shows the histograms of particle diameter distributions for films annealed at 500°C, 750°C and 800°C respectively.

The results of the EDS analysis carried out on the films to determine elemental composition and the presence of possible impurities are shown in Fig. 3. The results indicated the presence of iron (Fe), oxygen (O), tin (Sn) and silicon (Si). The Fe and O detected are the elemental composition of hematite. The tin oxide (SnO_2) in FTO is the source of Sn observed in our analysis. The Si detected resulted from the elemental composition of glass in glass/FTO substrates. A separate EDS investigation on glass/FTO substrate shown in Fig.3D indicated the presence of high amount of Si at about 2.5 keV. This confirmed the source of Si in the EDS analysis of our samples.

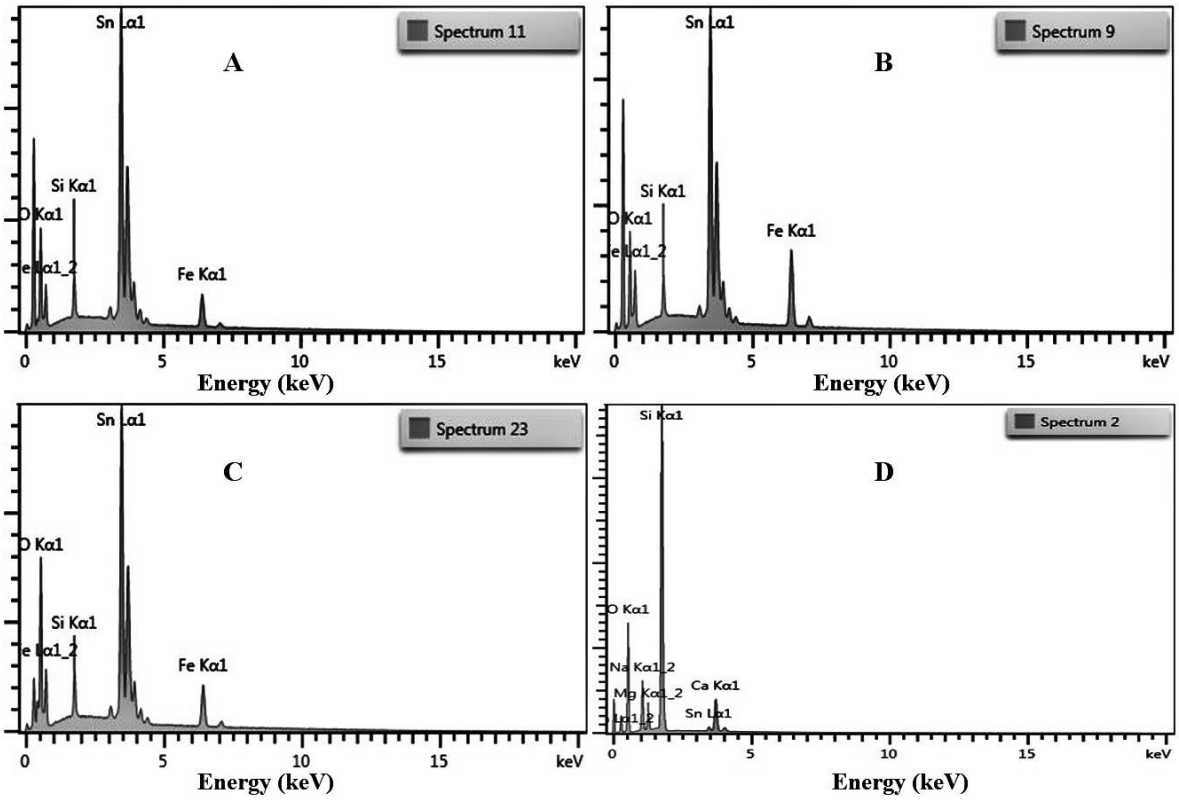

Fig. 3. EDS analysis of hematite films annealed at A) 500°C, B) 750°C, and C) 800°C; D) shows the analysis done on FTO.

3.1.2 Structural analysis

XRD was employed to study the structural properties of the hematite films. Fig. 4 presents the diffraction pattern. The diffraction peaks at (104), (110), (012), (113), (024), (122) and (310) planes corelate with those of rhombohedral crystal structure of hematite according to JCPDS no. 33-0664.

The films sintered at 750°C yielded the highest preferential growth in the (110) plane compared to other samples. For applications of hematite in photocatalysis, better conductivity and charge separation occurs more in the (110) plane [11]. Equation 3 shows the Debye-Scherrer relation employed to get the approximate crystal size of the films [23],

$$D = \frac{k\,\lambda}{\beta \cos\theta} \tag{3}$$

where k is 0.9 representing the estimated value of the shape factor, λ is 0.15418 nm representing the wavelength of the X-ray radiation used, β represents the full width at half maximum (FWHM) and θ is the Bragg angle. Table 1 presents the crystal sizes of the samples. The crystal size estimated for the films increases with annealing temperature up to 750°C. The maximum crystal size obtained is 45.9 nm for the hematite films sintered at 750°C, which is 82.9% higher than those of films annealed at 500°C with the least size. A slight drop in crystal size was observed with further annealing at 800°C relative to films annealed at 750°C. Possible deformation of FTO may have occurred at annealing temperature of 800°C which could

increase its resistance, thereby limiting crystallization of the films [17]. Enhanced crystallization can result in increased electron mobility in the films which is required for improved performance when applied towards photocatalysis [3].

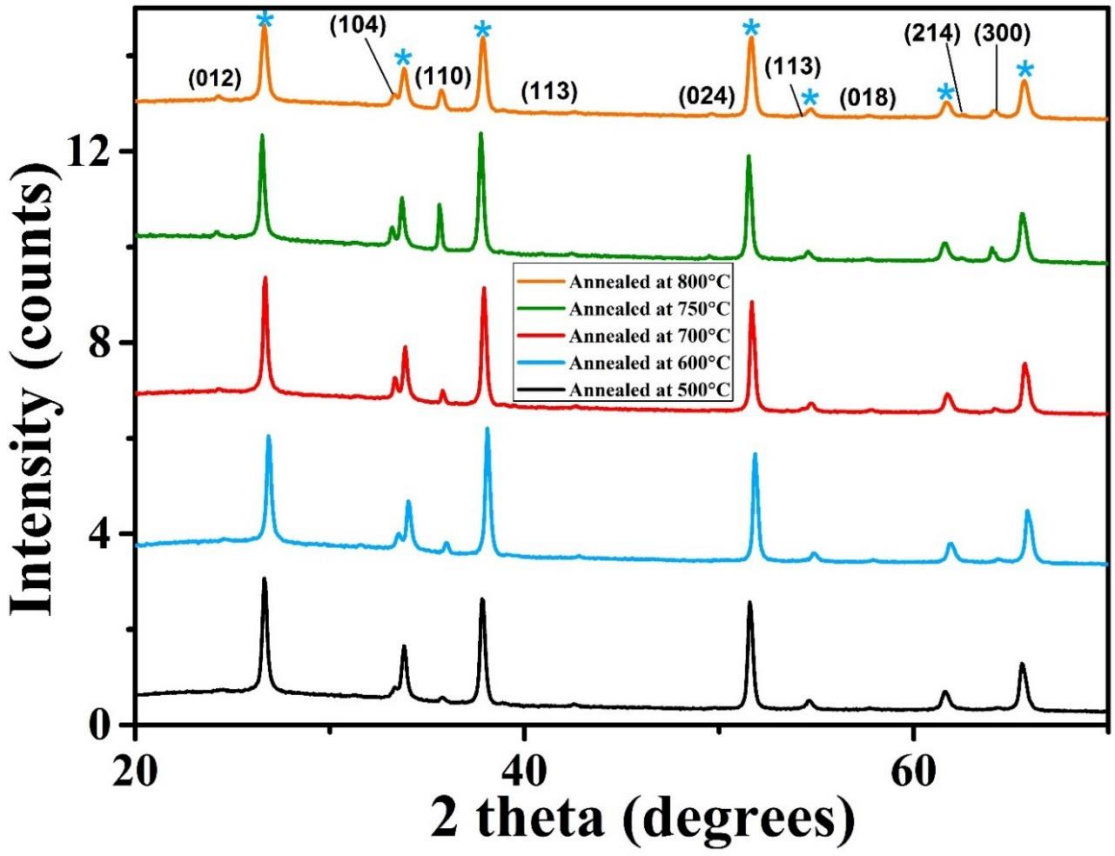

Fig. 4. XRD spectra of films annealed at 500°C, 600, 700°C, 750°C and 800°C respectively. The peaks labelled with * are those of FTO substrates.

In addition, the microstrain (e) and dislocation density (d) of the hematite films were estimated using $\varepsilon = \beta/4\tan\theta$ and $d = 1/D^2$ respectively [24], and the results are shown in Table 1. Decrease in strain and dislocation density was observed with increasing annealing temperature between 500-750°C. The dislocation density and microstrain for the films annealed at 750°C were 70% and 45% less than the values obtained for samples prepared at 500°C respectively. Reduction in microstrain and dislocation density with temperature is associated to decrease in grain boundaries and defect levels resulting from improved crystallization of the films [25]. Increasing annealing temperature to 800°C did not result in further lowering of dislocation density and microstrain.

Table 1. The results of XRD analysis for hematite films prepared under different annealing conditions.

Sample	Bragg angle (2θ)	FWHM (degrees)	Crystal size (nm)	Strain ε x 10^{-3}	Dislocation density ɖ x 10^{14} (Lin/$m^{2)}$
Annealed at 500°C	35.781	0.333	25.1	4.51	15.91
Annealed at 600°C	35.995	0.247	33.8	3.34	8.75
Annealed at 700°C	35.384	0.187	44.7	2.53	4.99
Annealed at 750°C	35.659	0.182	45.9	2.46	4.75
Annealed at 800°C	36.179	0.193	43.2	2.62	5.34

3.1.3 Optical properties

UV-Vis spectroscopy analysis was utilized to obtain information on the absorption, transmittance and optical band gap of hematite films prepared under different annealing conditions. Fig. 5 shows the transmittance spectra measured for all the films. The spectra showed decrease in transmittance with annealing temperature up to 750°C, at wavelengths below 550 nm. The increase in particle dimension of the nanostructures with annealing temperature decreases the number of scattering centres and increases the attenuation coefficient of light which led to the observed decrease in transmittance [26]. The inset in Fig. 5 shows more clearly the transmittance behaviour of the films at wavelengths below 550 nm. The drop in transmittance at wavelengths below 550°C nm was noticed for samples annealed at 800°C relative to the ones sintered at 750°C. The films annealed at 800°C appeared to be more reflective based on visual inspection which may have led to the decrease in transmittance observed.

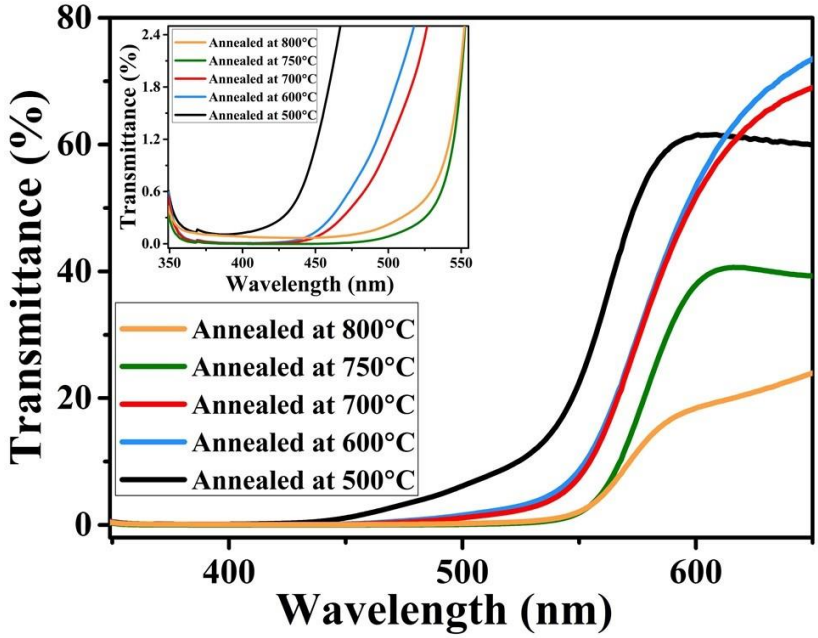

Fig. 5. UV-Vis transmittance spectra of hematite films prepared under different annealing conditions with an expanded view shown in the inset.

The absorption coefficient of the hematite films between wavelengths of 350-700 nm are shown in Fig. 6. The absorption coefficient (α) was estimated using the equation $\alpha = (2.304 \times A)/d$ [27], where A represents the absorbance while d stands for the film thickness approximated from FE-SEM cross-sectional images. The absorption coefficient for the films increases with annealing temperature with the best values observed for films treated at 750°C. The absorption coefficients of the films are in agreement with their transmittance spectra shown in Fig. 5. Improved absorption coefficient can improve photon absorption and photocatalytic performance of nanostructured films when applied towards water splitting.

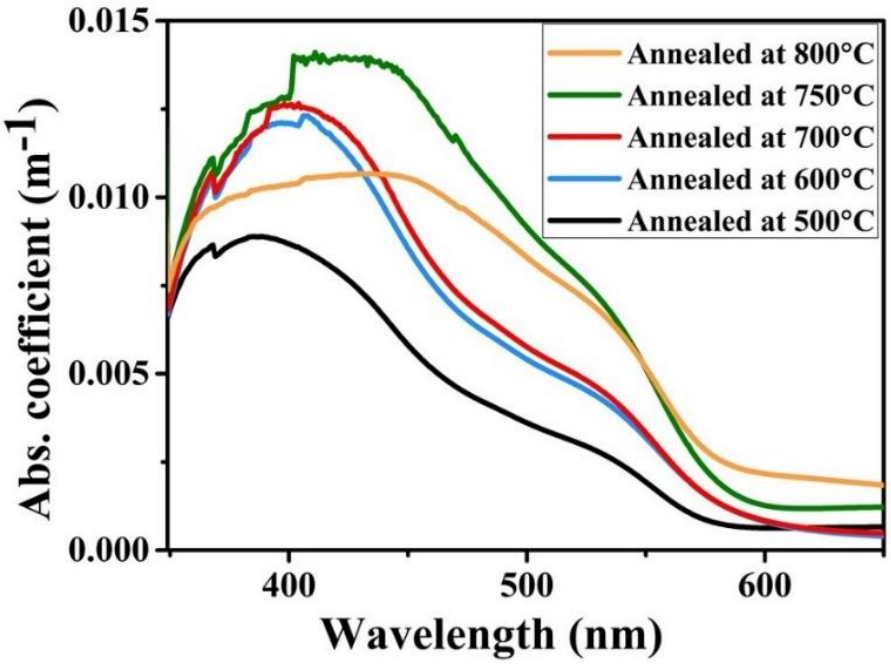

Fig. 6. Absorption coefficient spectra of hematite films prepared under different annealing conditions

The TAUC relation shown in equation 4 was employed to estimate the optical band gap of the films [28],

$$\alpha h\nu = A\left(h\nu - E_g\right)^n \qquad (4)$$

where h represent the Planck constant, ν stands for the frequency of light, A represents an arbitrary constant, E_g denote the band gap and n is a constant which is equals 2 for allowed indirect transitions and 1/2 for direct transitions. The indirect transitions have been linked to the spin-forbidden Fe^{3+} 3d to 3d excitation and the direct transitions are as a result of O^{2-} 2p to Fe^{3+} 3d charge transfer [29]. The graph of $(\alpha h\nu)^{1/2}$ against $h\nu$ shown in Fig. 7a was plotted and the linear portion of the curve was extrapolated to intersect the $h\nu$-axis and the value obtained represents the indirect band gap of the films. The direct band gap of the films was also obtained in a similar way from the plot of $(\alpha h\nu)^2$ against $h\nu$ shown in Fig. 7b. The indirect band gap estimated for the films reduces with annealing temperature and ranges from 1.93-2.00 eV. This agrees well with the values of indirect band gap reported for hematite in literature [30, 31]. The

estimated direct band gap of the films decreases with annealing temperature and ranges from 2.22-2.6 eV, similar to values that have been reported for hematite films [29, 32]. The band gap decrease with annealing temperature will improve light absorption in the visible region which could help in enhancing their performance during photocatalysis [33].

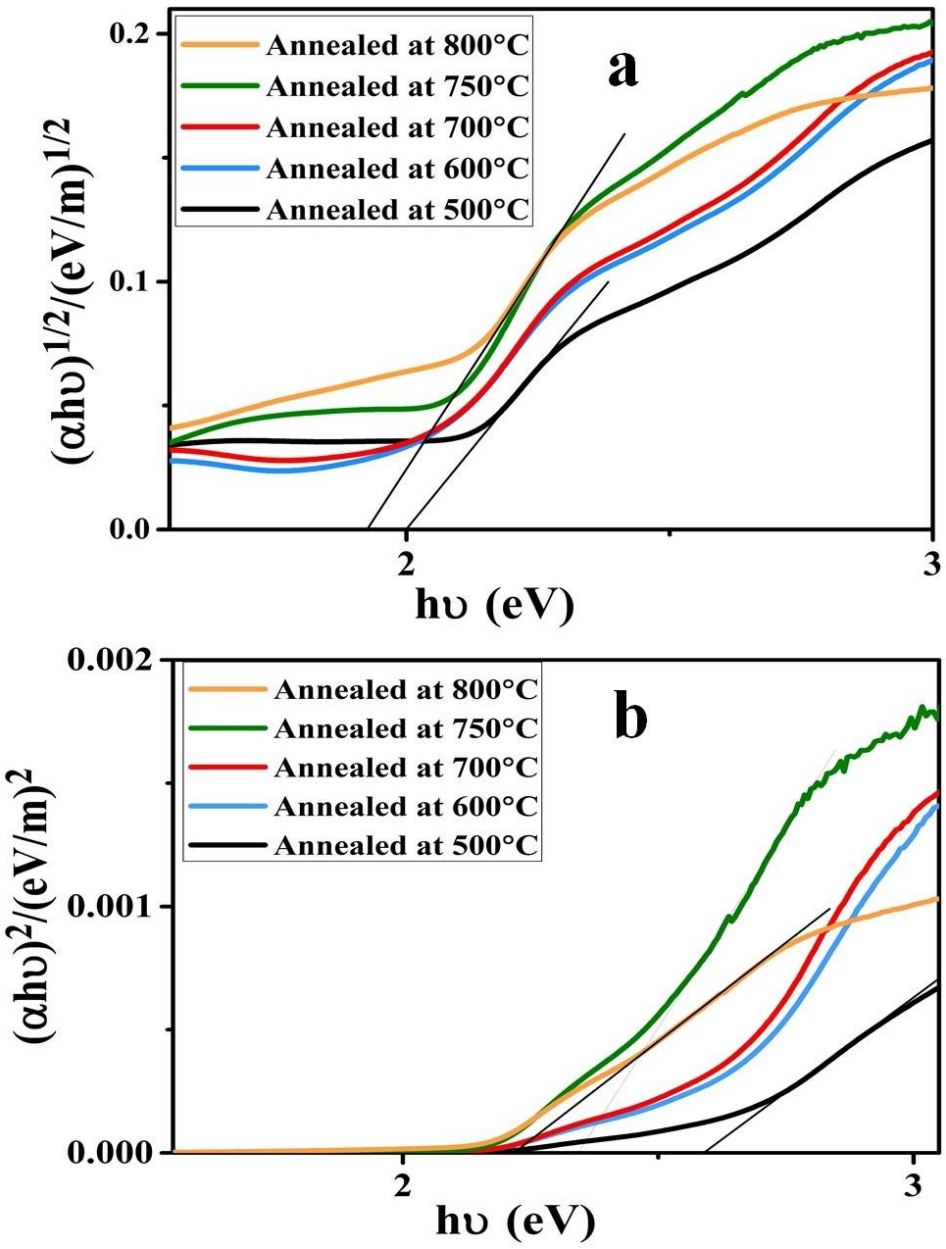

Fig. 7. Tauc plots for a) indirect bandgaps and b) direct bandgaps of the hematite films.

3.1.4 Resistivity measurements

The resistivity of FTO substrates were obtained using the linear four-point probe after annealing under the same conditions as the hematite films produced and the results are shown in Fig. 8. There was no notable increase in the resistivity of the substrates annealed between 500-750°C. However, further annealing at 800°C led to a drastic increase in the resistivity of the FTO substrates which was 7.7 times more than those of films sintered at 750°C. This

suggest that the FTO substrates used while preparing hematite films at 800°C may have suffered some deformation which could greatly affect film formation. The deformation of FTO substrates during deposition of hematite films annealed at 800°C resulted in decreased film crystallization relative to the ones treated at 750°C as earlier inferred in section 3.1.2.

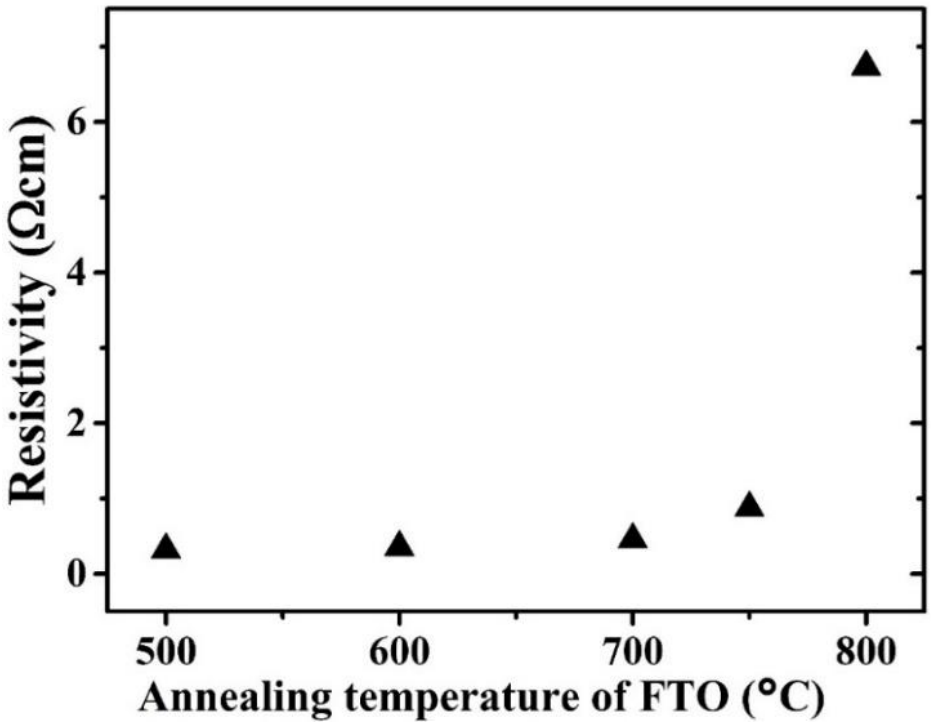

Fig. 8. Resistivity of FTO substrates after subjecting them to the same annealing conditions as the hematite films prepared.

3.2 Photoelectrochemical (PEC) performance

3.2.1 Linear sweep voltammetry

Linear sweep voltammetry was performed in dark and under illumination to obtain the photocurrent and onset potential of the films under 1 sun and the results are shown in Fig. 9. Photocurrent of 3.5×10^{-2} mA/cm^2 at 1.23 vs RHE and onset potential of 1.0 V vs RHE was observed for the films annealed at 500°C. Annealing of the last layer of the films at 600°C did not result in increased PEC performance for both photocurrent and onset potential shift. Increased photocurrent was recorded for films annealed at temperatures between 700-800°C. The maximum photocurrent of 1.9×10^{-1} mA/cm^2 at 1.23 V vs RHE was obtained for films annealed at 750°C which was over 5 times more than those of films sintered at 500°C, and the onset potential yielded a cathodic shift of 300 mV. This enhanced performance could be attributed to the high crystallization and absorption coefficients of films annealed at 750°C as observed in XRD and UV-Vis analysis shown in Fig. 4 and Fig. 6 respectively. Improved absorption coefficient will enhance the number of photons absorbed by the films (equation 4) while high crystallization reduces grain boundaries and improve electron mobility [3], leading to enhanced PEC performance. Annealing at 800°C did not result in further increase in performance, instead, there was an approximate of 17% drop in photocurrent at 1.23 V vs RHE

relative to the maximum value obtained for films annealed at 750°C. The decrease in absorption coefficient and the reduced crystal size for films annealed at 800°C may have contributed to the drop in PEC performance. Also, the deformation of FTO substrate (Fig. 8), lead to increased series resistance between FTO and α-Fe_2O_3 and this may have contributed to the decrease in photocurrent observed for films annealed at 800°C.

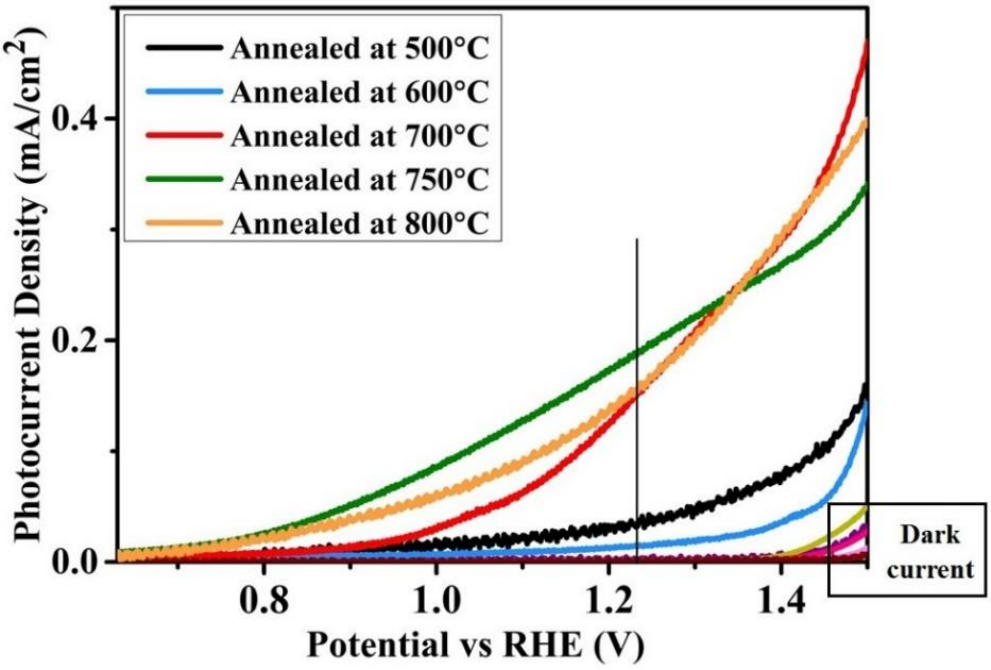

Fig. 9. Photocurrent densities of the hematite films prepared at different annealing conditions.

3.2.2 Mott-Schottky analysis

Mott-Schottky measurements were carried out to obtain the flat band potential (V_{fb}) and donor density (N_D) values for the films. The Mott-Schottky plots obtained for the films are shown in Fig. 10. The Mott-Schottky relation in equation 5 was utilized to estimate the donor densities and flat band potentials of the hematite films,

$$\frac{1}{C^2} = \frac{2}{\varepsilon_0 \varepsilon e A^2 N_D} \left(V - V_{fb} - \frac{KT}{e}\right) \quad (5)$$

where *C* represents the interfacial capacitance, *A* stands for the surface area of the electrode, ε is the dielectric constant given as 80 for hematite, ε_0 stands for the permittivity of free space, *e* represents the charge of an electron, *V* is the applied potential, K is the Boltzmann constant and T represents the temperature [34].

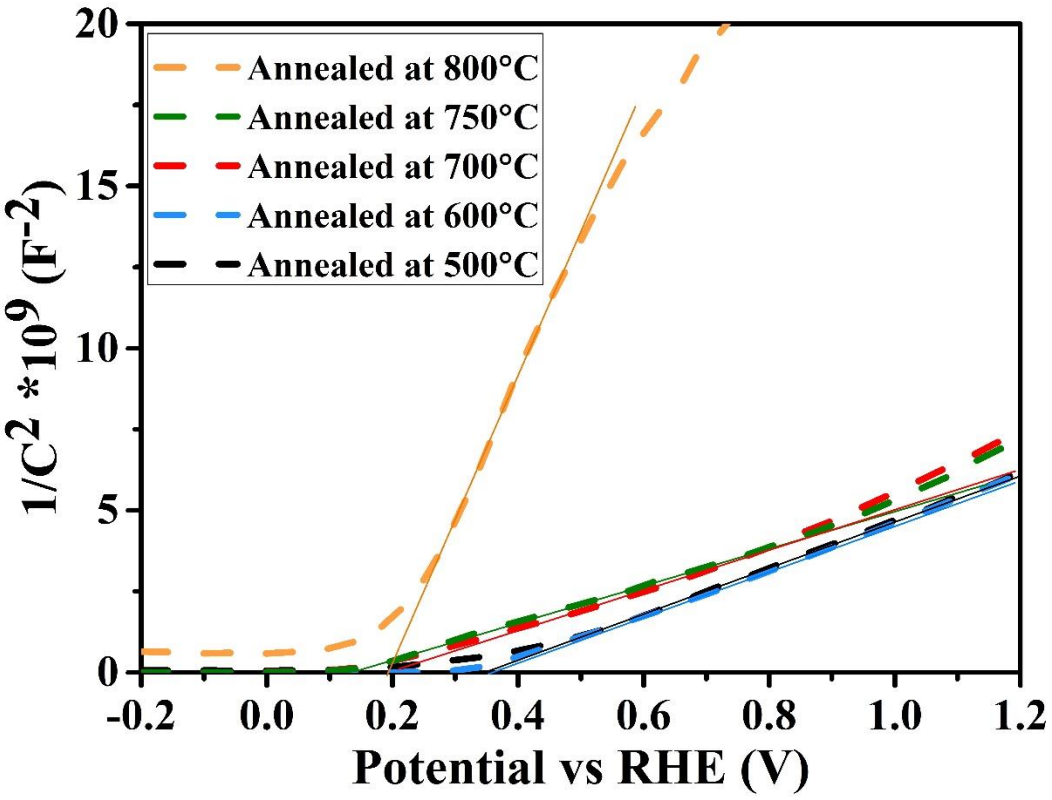

Fig. 10. Mott-Schottky plots of hematite films prepared under different annealing conditions.

The linear portions of the Mott-Schottky plots were fitted and the slope (S) of the plots was used to obtain N_D values for the samples according to the relation $S = 2/\varepsilon_0 \varepsilon e A^2 N_D$, extracted from equation 5. The positive slope obtained were expected for hematite films being n-type semiconductors [24]. The linear portion of the plots were extended to intercept the potential V_0 along V axis where $\frac{1}{C^2} = 0$. This simplifies equation 5 to $V_0 = V_{fb} + (KT/e)$ where the values for V_{fb} can be obtained. The estimated values of N_D and V_{fb} for all the hematite films are given in Table 2.

Table 2. Estimated values of flat band potential (V_{fb}) and donor density (N_D) of the hematite films prepared at different annealing conditions.

Sample	Flat band potential (V_{fb}) / V	$N_D \times 10^{19}$ /cm^{-3}
Annealed at 500°C	0.333	8.6
Annealed at 600°C	0.324	8.7
Annealed at 700°C	0.195	9.4
Annealed at 750°C	0.133	10.3
Annealed at 800°C	0.172	1.4

The V_{fb} values of the films decreases with annealing temperature up to 750°C. The films annealed at 750°C has a minimum V_{fb} of 0.13 V vs RHE which was 0.2 V less than the value obtained for films annealed at 500°C. The decrease in V_{fb} for films treated at 750°C can be

linked to the improved onset potential observed. Further annealing of the films at 800°C resulted in a slight increase of about 0.04 V in V_{fb} compared with those annealed at 750°C. The V_{fb} values in this study are similar to what was obtained for hematite films elsewhere [24]. A correlation was observed between the onset and flat band potential during photocurrent measurements. The onset potential for the films decreases with reduction of V_{fb} leading to improved PEC performance in terms of the potential required for oxygen evolution reaction (OER). This observation agrees with a previous study that related a drop in V_{fb} with lowering of onset potential [31, 35]. Another correlation between the crystal sizes of the films estimated from XRD analysis and V_{fb} values obtained was observed. Increase in the crystal size of the films resulted in lowering of V_{fb} as seen in Fig. 11. This may be due to the reduction in the density of grain boundaries with crystal size increase, thus lowering the resistance in the films, leading to decrease of V_{fb} values [31].

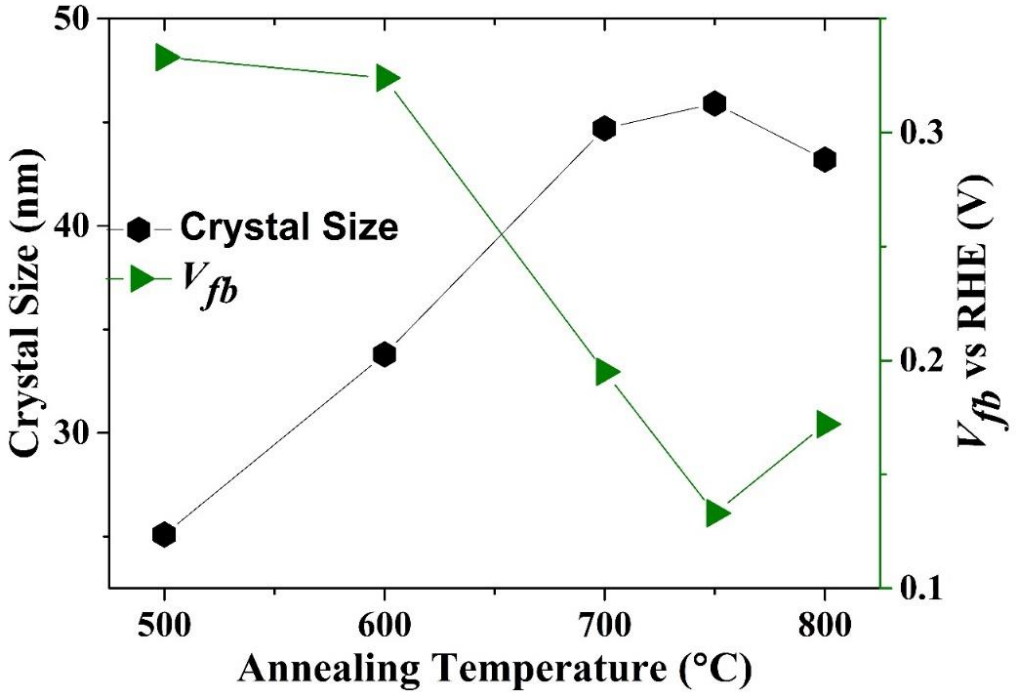

Fig. 11. Correlation between the crystal sizes estimated from XRD analysis and flat band potentials (V_{fb}) of the hematite films annealed at different annealing conditions.

The N_D values estimated for the films are in the order of 10^{19} cm^{-3} and compares closely with what has been obtained in literature for hematite [36, 37]. The N_D values increases with annealing temperature to a maximum of 10.3×10^{19} cm^{-3} for films annealed at 750°C. We attributed two possible causes for the observed increase in N_D with temperature. First, reduction in the density of grain boundaries with annealing temperature may have resulted in improved conductivity of the films and could have led to the observed increase in N_D [31]. Secondly, unintentional doping of hematite from Sn content of FTO through diffusion at elevated annealing temperature has been reported [37, 38], which can also result in increased N_D values. Although we cannot rule out the possibility of unintentional Sn doping, however, the magnitude of increase in the N_D value was only by a maximum factor of 1.2. For this reason, the increase in N_D value recorded could largely be due to the lowering of grain boundary

densities with temperature as a result of improve crystallization. The increase in N_D value for films annealed at 750°C contributed to the enhanced photocurrent that was observed for the samples. A drop in N_D was recorded for films annealed at 800°C and we attributed this to the deformation of the FTO substrates, and increase in the resistance of films produced due to possible aggregation of the hematite nanoparticles [38].

Electrochemical impedance spectroscopy (EIS) studies

EIS studies was done to investigate the impact of the modified annealing approach on charge transport kinetics in the bulk and surface of the hematite photoanodes. The Nyquist plots of the EIS study done under illumination are shown in Fig. 12 with the inset showing the equivalent circuit used to fit the experimental data. The circuit element Rs denote the series resistance linked to the FTO/hematite contact, the external wire connections and the electrolyte's ionic conductivity [39]. Rb denote the charge trapping resistance in the bulk of the films, constant phase element 1 (CPE1) represents the bulk capacitance of the space charge region, Rct is the resistance to charge transfer from the surface of the films to the conducting electrolyte and CPE2 represents the capacitance of the surface states [40-42]. CPE elements were used to represent the capacitance of the films since the semicircles obtained in the Nyquist plots for the films appeared to be depressed, an indication of non-ideal capacitive behaviour [43]. The values recorded for the circuit elements are shown in Table 3.

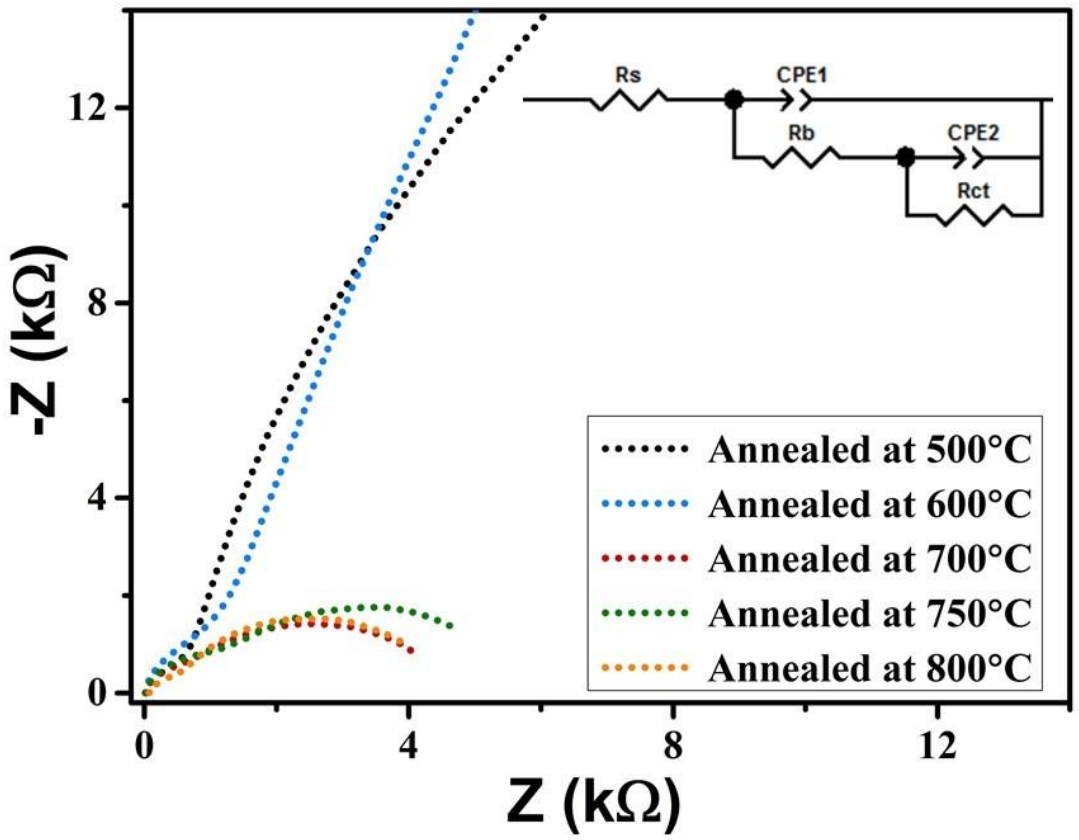

Fig. 12. EIS Nyquist plots of hematite thin film prepared under different annealing conditions with the inset showing the modelled circuit used in fitting the experimental data.

Table 3. The estimated values recorded for equivalent circuit elements after fitting the experimental data obtained from EIS analysis of hematite films.

Sample	Rs (Ω)	R1 (kΩ)	CPE1 (µF)	R2 kΩ	CPE2 (µF)
Annealed at 500°C	11.07	1.24	27.91	70.99	49.54
Annealed at 600°C	11.27	2.17	21.11	183.28	58.312
Annealed at 700°C	16.22	1.10	16.81	3.50	105.30
Annealed at 750°C	32.78	1.66	22.81	3.88	170.51
Annealed at 800°C	68.57	1.55	70.19	3.15	45.24

The series resistance Rs associated with the FTO/hematite contact increases with the annealing temperature of the samples. Films annealed at 800°C had the highest series resistance of 68.57 Ω which was over 6 times more than the value obtained for films sintered at 500°C. This agrees with the resistivity measurements discussed in section 3.1.4 which yielded the highest resistance for FTO substrates annealed at 800°C. The charge trapping resistance Rb in the bulk of the films was in the range of (1.10 - 2.17) kΩ with films annealed at 600°C having the highest value. Annealing of last layers of the films at elevated temperatures did not yield a noticeable decrease in the bulk resistance Rb of the films. Also, the bulk capacitance in the space charge region did not improve with annealing temperature except for films annealed at 800°C which shows a 2.5-fold increase relative to the ones annealed at 500°C. Low trapping resistance and high capacitance values in the bulk of the films can help improve the transport of photogenerated holes to the surface of the hematite photoanodes for oxidation water.

The electrochemical properties at the surface of the hematite films was noticeably influenced by annealing the last layers of the films at elevated temperatures. The resistance to charge transfer Rct, at the surface of the photoanodes was notably reduced for films annealed at temperatures above 700°C, yielding values in the range of 3.15-3.88 kΩ compared to the 70 kΩ recorded for films annealed at 500°C. This implies that films annealed above 700°C are more likely to inject holes from their valence bands into the electrolyte through surface states instead of experiencing bulk recombination with electrons, thereby improving PEC performance [40]. This is in line with the improve photocurrent recorded for films annealed above 700°C as seen in Fig. 9. Films annealed at 600°C yielded a high Rct value of 183.28 kΩ, which is largely the reason behind the low photocurrent obtained for the film. The surface states capacitance CPE2 increased for films annealed at 700°C and 750°C compared to the ones sintered at 500°C. Increase in surface states capacitance indicates the ability of the photoanodes to accumulate more charges at their surface which is crucial for water oxidation [42, 44]. The films annealed at 750°C recorded the highest surface states capacitance which may be one of the reasons why it recorded the best photocurrent at 1.23 V vs RHE. The photocurrent of films annealed at 800°C was less than the value recorded for films annealed at 750°C despite having a slightly lower Rct. This is because of the low surface states capacitance recorded for films annealed at 800°C and its high series resistance Rs associated with the FTO/hematite contact which will limit flow of electrons from the photoanode to the cathode through the back-contact [45].

4 Conclusion

Multi-layered hematite thin films consisting of four layers were prepared on FTO substrates by annealing the first three layers at 500°C and the impact of treating the last layers at 500, 600,

700, 750 and 800°C on the PEC performance of the films was investigated. Films annealed at 700°C and above yielded improve PEC performance. The films annealed at 750°C yielded the best performance with photocurrent of 0.19 mA/cm^2 at 1.23 V vs RHE which was 5.3 times more than what was obtained for films annealed at 500°C, and the onset potential shifted cathodically by 300 mV. Improved crystallization and the preferential growth in the (110) plane for films annealed at 750°C as observed in XRD analysis contributed to the enhanced performance. Improved absorption coefficients for films annealed at 750°C also allows for more photon absorption which may have contributed to the enhanced performance observed. Mott-Schottky analysis reveals additional reasons for the improved PEC performance observed for films annealed at 750°C. The films recorded the least flat band potential of 0.13 V vs RHE which caused the cathodic shift in the onset potential observed. Also, the donor density for the films sintered at 750°C improved by a maximum factor of 1.2 relative to those annealed at 500°C which also contributed in the enhanced photocurrent observed. EIS studies shows that the reduced charge transfer resistance at the hematite/electrolyte interface couple with increased capacitance of surface states contributes to the enhanced PEC performance recorded for films annealed at 750°C. Further annealing the films at 800°C resulted in a drop in PEC performance which is attributed to the deformation of FTO substrates and reduced capacitance of the surface states relative to the ones treated at 750°C. This study reveals that the performance of multi-layered hematite films could be enhanced by annealing the last layers at elevated temperatures without any significant damage to the conducting substrates and consequently improving the photocurrent.

Acknowledgements

The authors acknowledge funding from the National Research Foundation - The World Academy of Sciences (NRF-TWAS), grant UID; 110814, the University of Pretoria, South African Research Chairs Initiative (SARCHI), UID; 115463. We also acknowledge funding from NRF N00500, UID; 112085 (NRF Research Development Grant), project UID; 110983 (Blue Skies Research Programme) and the CSIR National Laser Centre Rental Pool Programme towards the purchase of VersaStat 3F potentiostat used in this project.

References

[1] K. Sivula, F. Le Formal, M. Grätzel, Solar water splitting: progress using hematite (α-Fe_2O_3) photoelectrodes, ChemSusChem, 4 (2011) 432-449.
[2] P. Liao, E.A. Carter, Hole transport in pure and doped hematite, Journal of Applied Physics, 112 (2012) 013701.
[3] T. Schuler, M.A. Aegerter, Optical, electrical and structural properties of sol gel ZnO: Al coatings, Thin Solid Films, 351 (1999) 125-131.
[4] Y. Ohya, H. Saiki, T. Tanaka, Y. Takahashi, Microstructure of TiO, and ZnO Films Fabricated by the, J. Am. Ceram. Soc, 79 (1996) 825-830.
[5] M.A. Aegerter, A. Reich, D. Ganz, G. Gasparro, J. Pütz, T. Krajewski, Comparative study of SnO_2: Sb transparent conducting films produced by various coating and heat treatment techniques, Journal of non-crystalline solids, 218 (1997) 123-128.
[6] Y. Takahashi, S. Okada, R.B.H. Tahar, K. Nakano, T. Ban, Y. Ohya, Dip-coating of ITO films, Journal of non-crystalline solids, 218 (1997) 129-134.

[7] C. Zhang, Q. Wu, X. Ke, J. Wang, X. Jin, S. Xue, Ultrathin hematite films deposited layer-by-layer on a TiO2 underlayer for efficient water splitting under visible light, International Journal of Hydrogen Energy, 39 (2014) 14604-14612.
[8] K. Gajda-Schrantz, S. Tymen, F. Boudoire, R. Toth, D.K. Bora, W. Calvet, M. Grätzel, E.C. Constable, A. Braun, Formation of an electron hole doped film in the α-Fe 2 O 3 photoanode upon electrochemical oxidation, Physical Chemistry Chemical Physics, 15 (2013) 1443-1451.
[9] R.H. Gonçalves, B.H. Lima, E.R. Leite, Magnetite colloidal nanocrystals: A facile pathway to prepare mesoporous hematite thin films for photoelectrochemical water splitting, Journal of the American Chemical Society, 133 (2011) 6012-6019.
[10] D.K. Bora, A. Braun, S. Erat, A.K. Ariffin, R. Löhnert, K. Sivula, J.r. Töpfer, M. Grätzel, R. Manzke, T. Graule, Evolution of an oxygen near-edge X-ray absorption fine structure transition in the upper Hubbard band in α-Fe2O3 upon electrochemical oxidation, The Journal of Physical Chemistry C, 115 (2011) 5619-5625.
[11] N.M. Ito, W.M. Carvalho, D.N.F. Muche, R.H.R. Castro, G.M. Dalpian, F.L. Souza, High temperature activation of hematite nanorods for sunlight driven water oxidation reaction, Physical Chemistry Chemical Physics, 19 (2017) 25025-25032.
[12] T.J. LaTempa, X. Feng, M. Paulose, C.A. Grimes, Temperature-dependent growth of self-assembled hematite (α-Fe2O3) nanotube arrays: rapid electrochemical synthesis and photoelectrochemical properties, The Journal of Physical Chemistry C, 113 (2009) 16293-16298.
[13] B.L. Bennett, E.C. Wyatt, C.T. Harris, Fabrication of thickness-controlled hematite thin films via electrophoretic deposition and subsequent heat treatment of pyridine-capped maghemite nanoparticles, Industrial & Engineering Chemistry Research, 55 (2016) 11583-11588.
[14] J.A. Klug, N.G. Becker, S.C. Riha, A.B. Martinson, J.W. Elam, M.J. Pellin, T. Proslier, Low temperature atomic layer deposition of highly photoactive hematite using iron (III) chloride and water, Journal of Materials Chemistry A, 1 (2013) 11607-11613.
[15] S. Jiao, L. Xu, K. Hu, J. Li, S. Gao, D. Xu, Morphological control of α-FeOOH nanostructures by electrodeposition, The Journal of Physical Chemistry C, 114 (2009) 269-273.
[16] P.S. Shinde, A. Annamalai, J.Y. Kim, S.H. Choi, J.S. Lee, J.S. Jang, Fine-tuning pulse reverse electrodeposition for enhanced photoelectrochemical water oxidation performance of α-Fe2O3 photoanodes, The Journal of Physical Chemistry C, 119 (2015) 5281-5292.
[17] J.Y. Kim, G. Magesh, D.H. Youn, J.-W. Jang, J. Kubota, K. Domen, J.S. Lee, Single-crystalline, wormlike hematite photoanodes for efficient solar water splitting, Scientific reports, 3 (2013) 2681.
[18] P.I. Kyesmen, N. Nombona, M. Diale, Influence of coating techniques on the optical and structural properties of hematite thin films, Surfaces and Interfaces, 17 (2019) 100384.
[19] A.G. Tamirat, A.A. Dubale, W.-N. Su, H.-M. Chen, B.-J. Hwang, Sequentially surface modified hematite enables lower applied bias photoelectrochemical water splitting, Physical Chemistry Chemical Physics, 19 (2017) 20881-20890.
[20] Y. Caglar, S. Ilican, M. Caglar, F. Yakuphanoglu, J. Wu, K. Gao, P. Lu, D. Xue, Influence of heat treatment on the nanocrystalline structure of ZnO film deposited on p-Si, Journal of Alloys and Compounds, 481 (2009) 885-889.
[21] N. Raship, M. Sahdan, F. Adriyanto, M. Nurfazliana, A. Bakri, Effect of annealing temperature on the properties of copper oxide films prepared by dip coating technique, in: AIP Conference Proceedings, AIP Publishing, 2017, pp. 030121.

[22] Y.W. Phuan, M.N. Chong, T. Zhu, S.-T. Yong, E.S. Chan, Effects of annealing temperature on the physicochemical, optical and photoelectrochemical properties of nanostructured hematite thin films prepared via electrodeposition method, Materials Research Bulletin, 69 (2015) 71-77.
[23] M. Zhu, Y. Wang, D. Meng, X. Qin, G. Diao, Hydrothermal synthesis of hematite nanoparticles and their electrochemical properties, The Journal of Physical Chemistry C, 116 (2012) 16276-16285.
[24] Z. Landolsi, I.B. Assaker, R. Chtourou, S. Ammar, Photoelectrochemical impedance spectroscopy of electrodeposited hematite α-Fe 2 O 3 thin films: effect of cycle numbers, Journal of Materials Science: Materials in Electronics, 29 (2018) 8176-8187.
[25] A. Begum, A. Hussain, A. Rahman, Effect of deposition temperature on the structural and optical properties of chemically prepared nanocrystalline lead selenide thin films, Beilstein journal of nanotechnology, 3 (2012) 438-443.
[26] M. Baikov, A. Ponyavina, A. Prishivalko, V. Sviridov, N. Sil'Vanovich, Effect of the microstructure of closely packed ultradisperse hematite layers on their spectral properties, Journal of applied spectroscopy, 63 (1996) 297-303.
[27] A. Shirzadi, A. Nezamzadeh-Ejhieh, Enhanced photocatalytic activity of supported CuO–ZnO semiconductors towards the photodegradation of mefenamic acid aqueous solution as a semi real sample, Journal of Molecular Catalysis A: Chemical, 411 (2016) 222-229.
[28] S. Li, J. Cai, Y. Mei, Y. Ren, G. Qin, Thermal oxidation preparation of doped hematite thin films for photoelectrochemical water splitting, International Journal of Photoenergy, 2014 (2014).
[29] F.L. Souza, K.P. Lopes, P.A. Nascente, E.R. Leite, Nanostructured hematite thin films produced by spin-coating deposition solution: Application in water splitting, Solar energy materials and solar cells, 93 (2009) 362-368.
[30] E.L. Tsege, T.S. Atabaev, M.A. Hossain, D. Lee, H.-K. Kim, Y.-H. Hwang, Cu-doped flower-like hematite nanostructures for efficient water splitting applications, Journal of Physics and Chemistry of Solids, 98 (2016) 283-289.
[31] B. Iandolo, H. Zhang, B. Wickman, I. Zorić, G. Conibeer, A. Hellman, Correlating flat band and onset potentials for solar water splitting on model hematite photoanodes, RSC Advances, 5 (2015) 61021-61030.
[32] E.L. Miller, D. Paluselli, B. Marsen, R.E. Rocheleau, Low-temperature reactively sputtered iron oxide for thin film devices, Thin Solid Films, 466 (2004) 307-313.
[33] H. Wang, J.A. Turner, Characterization of hematite thin films for photoelectrochemical water splitting in a dual photoelectrode device, Journal of The Electrochemical Society, 157 (2010) F173-F178.
[34] Y. Liang, C.S. Enache, R. van de Krol, Photoelectrochemical Characterization of Sprayed, International Journal of Photoenergy, 2008 (2008).
[35] P.S. Shinde, S.H. Choi, Y. Kim, J. Ryu, J.S. Jang, Onset potential behavior in α-Fe 2 O 3 photoanodes: the influence of surface and diffusion Sn doping on the surface states, Physical Chemistry Chemical Physics, 18 (2016) 2495-2509.
[36] B. Wickman, A.B. Fanta, A. Burrows, A. Hellman, J.B. Wagner, B. Iandolo, Iron oxide films prepared by rapid thermal processing for solar energy conversion, Scientific reports, 7 (2017) 40500.
[37] L.P. de Souza, R.O. Chaves, A. Malachias, R. Paniago, S.O. Ferreira, A.S. Ferlauto, Influence of annealing temperature and Sn doping on the optical properties of hematite thin films determined by spectroscopic ellipsometry, Journal of Applied Physics, 119 (2016) 245104.

[38] E.S. Cho, M.J. Kang, Y.S. Kang, Enhanced photocurrent density of hematite thin films on FTO substrates: effect of post-annealing temperature, Physical Chemistry Chemical Physics, 17 (2015) 16145-16150.
[39] T. Lopes, L. Andrade, F. Le Formal, M. Gratzel, K. Sivula, A. Mendes, Hematite photoelectrodes for water splitting: evaluation of the role of film thickness by impedance spectroscopy, Physical Chemistry Chemical Physics, 16 (2014) 16515-16523.
[40] P.S. Bassi, L. Xianglin, Y. Fang, J.S.C. Loo, J. Barber, L.H. Wong, Understanding charge transport in non-doped pristine and surface passivated hematite (Fe 2 O 3) nanorods under front and backside illumination in the context of light induced water splitting, Physical Chemistry Chemical Physics, 18 (2016) 30370-30378.
[41] A.Y. Ahmed, M.G. Ahmed, T.A. Kandiel, Hematite photoanodes with size-controlled nanoparticles for enhanced photoelectrochemical water oxidation, Applied Catalysis B: Environmental, 236 (2018) 117-124.
[42] B. Eftekharinia, A. Moshaii, A. Dabirian, N.S. Vayghan, Optimization of charge transport in a Co–Pi modified hematite thin film produced by scalable electron beam evaporation for photoelectrochemical water oxidation, Journal of Materials Chemistry A, 5 (2017) 3412-3424.
[43] N. Perini, A. Prado, C. Sad, E. Castro, M. Freitas, Electrochemical impedance spectroscopy for in situ petroleum analysis and water-in-oil emulsion characterization, Fuel, 91 (2012) 224-228.
[44] B. Klahr, S. Gimenez, F. Fabregat-Santiago, T. Hamann, J. Bisquert, Water oxidation at hematite photoelectrodes: the role of surface states, Journal of the American Chemical Society, 134 (2012) 4294-4302.
[45] N.D. Sankir, M. Sankir, Photoelectrochemical Solar Cells, John Wiley & Sons, 2018.